

## Application of the R-matrix method to Photoionization of Molecules

Motomichi TASHIRO (田代基慶)<sup>1, a)</sup>

*Institute for Molecular Science, Nishigo-Naka 38, Myodaiji, Okazaki 444-0867,  
Japan*

(Dated: 22 May 2018)

The R-matrix method has been used for theoretical calculation of electron collision with atoms and molecules for long years. The method was also formulated to treat photoionization process, however, its application has been mostly limited to photoionization of atoms. In this work, we implement the R-matrix method to treat molecular photoionization problem based on the UK R-matrix codes. This method can be used for diatomic as well as polyatomic molecules, with multi-configurational description for electronic states of both target neutral molecule and product molecular ion. Test calculations were performed for valence electron photoionization of nitrogen ( $\text{N}_2$ ) as well as nitric oxide (NO) molecules. Calculated photoionization cross sections and asymmetry parameters agree reasonably well with the available experimental results, suggesting usefulness of the method for molecular photoionization.

---

<sup>a)</sup>E-mail:tashiro@ims.ac.jp

## I. INTRODUCTION

Photoionization of molecule has been studied for long year because of its importance in modeling and understanding upper atmosphere, interstellar clouds and industrial plasma. Photoionization process has also been used to understand nature of molecular electronic states as well as dynamics of nuclei on excited electronic state<sup>1</sup>. In addition to the conventional measurement of integral cross section and photoelectron asymmetry parameter for randomly oriented molecule, recent developments of experimental technique have made it possible to extract photoelectron angular distribution from oriented molecule<sup>2</sup>, perform accurate measurement of inner-shell photoionization cross section<sup>3</sup>.

Several theoretical methods have been developed for treating photoionization of molecule, based on the Schwinger variational principle<sup>4</sup>, random phase approximation<sup>5,6</sup>, time-dependent density functional theory<sup>7</sup>, complex basis function<sup>8,9</sup>, Stieltjes imaging method<sup>10</sup>, and so on. These methods have successfully reproduced or predicted experimental results for photoionization of small to medium sized molecules in the gas phase.

The R-matrix method, originally developed for nuclear reaction<sup>11</sup>, has been applied for accurate calculation of cross section for electron collision with atoms, molecules and ions with great success<sup>12-16</sup>. As the other electron scattering theories such as the Schwinger variational method<sup>4</sup> and the Kohn variational method<sup>17</sup>, the R-matrix method was also formulated to treat photoionization of atoms and molecules<sup>18</sup>. In addition to the single-photon ionization process, the method was also modified to treat multi-photon ionization process<sup>19,20</sup>. There have been many applications of the R-matrix method to photoionization of atoms<sup>12,18</sup>, however, its application to molecular photoionization has been fairly limited, with only a few reports on hydrogen molecule<sup>21,22</sup>. The ab initio R-matrix method can reproduce the existing experimental cross sections very well, as has been demonstrated in the previous electron-molecule scattering calculations<sup>23,24</sup>. Thus, the method is expected to work efficiently in molecular photoionization problem as well. Introduction of a different method, the R-matrix method, may be useful when various theoretical methods are compared with experiment. In the R-matrix treatment of photoionization, it is possible to represent electronic states of target molecular ion by multi-configurational wavefunctions, as it has been in the R-matrix calculations on electron molecule collisions<sup>12-16,23,24</sup>. This multi-configurational representation of wavefunction may be good for description of satellite

or resonance states with multi-configurational character, as well as introducing correlation in the initial and final states.

In this work, we implement the R-matrix method of molecular photoionization based on the work of Burke and Taylor<sup>18</sup> originally proposed for atomic photoionization. Our procedure is roughly divided into two stages. In the first stage, we perform R-matrix calculations for electron collision with molecular ion, and obtain eigenvalues and eigenvectors of the R-matrix eigenstates by diagonalizing the electronic Hamiltonian inside the R-matrix sphere. In the second stage, the initial and final state wavefunctions of photoionization are constructed as linear combinations of the R-matrix eigenstates obtained in the first stage, then the transition dipole moments between these initial and final state are obtained for calculation of photoionization cross section and asymmetry parameter. For calculation in the first stage, we use the polyatomic version of the UK R-matrix codes developed by Morgan et al.<sup>13</sup> The UK R-matrix codes has been successfully applied to many electron-molecule scattering problems in the past. In this work, some modifications are made to the UK R-matrix codes, e.g., to enable transition dipole moment calculation between the R-matrix eigenstates. In order to verify reliability and accuracy of the R-matrix method for molecular photoionization, cross sections and asymmetry parameters are calculated for valence electron photoionization of nitrogen ( $N_2$ ) and nitric oxide (NO) molecules randomly oriented in the gas phase, and the results are compared with existing experimental and theoretical data.  $N_2$  has been benchmark molecule for various theories of photoionization, and will be also good for the first test calculation of the R-matrix method for molecular photoionization. In contrast to  $N_2$  molecule, number of calculations on photoionization of NO molecule is limited<sup>25</sup>. We selected NO molecule as the second test case, to see capability of the method to treat this open-shell molecule with  $\Pi$  ground state.

## II. THEORETICAL METHOD

In this section, we describe the procedure to obtain molecular photoionization cross section and asymmetry parameter using the R-matrix method. Our discussion mainly follows Chandra<sup>26,27</sup> and Burke and Taylor<sup>18</sup>. Many equations in this section already appear in their papers, however, they are shown here for reader's convenience.

Differential cross section for photoionization of molecule randomly oriented in space can

be written as,<sup>26,27</sup>

$$\frac{d\sigma}{d\hat{\mathbf{k}}'} = \frac{3}{4} \left( \frac{e^2}{\alpha E_r} \right)^2 \sum_L A_L(k) P_L(\cos \theta'), \quad (1)$$

where  $\hat{\mathbf{k}}'$  represents direction of a photoelectron with wavenumber  $k$  in laboratory frame,  $E_r$  is photon energy,  $P_L$  is a Legendre polynomial,  $\theta'$  is the angle between the direction of photoelectron and the polarization vector of the incident photon. Here we assume that the photon beam is linearly polarized. The expansion coefficient  $A_L(k)$  is represented as

$$A_L(k) = (2L+1) \begin{pmatrix} 1 & 1 & L \\ 0 & 0 & 0 \end{pmatrix} \sum_{l_f m_f \lambda_r} \sum_{l'_f m'_f \lambda'_r} (-i)^{l_f - l'_f} e^{i(\sigma_{l_f} - \sigma_{l'_f})} (-1)^{m_f + \lambda_r} (2l_f + 1) (2l'_f + 1) \\ \times \begin{pmatrix} l_f & l'_f & L \\ 0 & 0 & 0 \end{pmatrix} \begin{pmatrix} l_f & l'_f & L \\ -m_f & m'_f & \epsilon \end{pmatrix} \begin{pmatrix} 1 & 1 & L \\ \lambda_r & -\lambda'_r & -\epsilon \end{pmatrix} M_{l_f m_f}^-(\lambda_r) M_{l'_f m'_f}^{-*}(\lambda'_r), \quad (2)$$

where  $l_f$ ,  $l'_f$ ,  $m_f$  and  $m'_f$  specify angular quantum number of the photoelectron associated with the final electronic state  $f$  of the product molecular ion,  $\epsilon$  equals to  $m_f - m'_f$ ,  $\sigma_{l_f}$  is the Coulomb phase, and  $M_{l_f m_f}^-(\lambda_r)$  represents transition dipole matrix element between the initial state  $\Psi_i$  and the final state  $\Psi_{l_f m_f}^{f-}$ ,

$$M_{l_f m_f}^-(\lambda_r) = A \langle \Psi_{l_f m_f}^{f-} | \sum_{s=1}^{n_e} \hat{\mathbf{e}}_{\lambda_r} \cdot \mathbf{r}_s | \Psi_i \rangle. \quad (3)$$

Here  $\hat{\mathbf{e}}_{\lambda_r}$  is the unit vector describing polarization  $\lambda_r$  of the incident photon in molecular frame,  $n_e$  is number of electrons in the system with  $\mathbf{r}_s$  being coordinates of the  $s$ th electron. In this work, we employ dipole length approximation. Thus, the proportional coefficient  $A$  becomes<sup>26</sup>  $(4\pi\alpha^3 E_r^3 / 3e^4)^{1/2}$  with  $\alpha$  being the fine structure constant. As is well known, the differential photoionization cross section in Eq. (1) can be simplified in the form,

$$\frac{d\sigma}{d\hat{\mathbf{k}}'} = \frac{\sigma_{tot.}}{4\pi} [1 + \beta P_2(\cos \theta')], \quad (4)$$

with the integrated cross section,

$$\sigma_{tot.} = \pi \left( \frac{e^2}{\alpha E_r} \right)^2 \sum_{l_f m_f \lambda_r} \left| M_{l_f m_f}^{f-}(\lambda_r) \right|^2, \quad (5)$$

and the asymmetry parameter,

$$\beta = \frac{A_{L=2}(k)}{A_{L=0}(k)}. \quad (6)$$

Following Burke and Taylor<sup>18</sup>, we evaluate the transition dipole matrix elements in Eq. (3) using the R-matrix method<sup>13-16</sup> for electron-molecule collision. In this method, configuration

space is divided by two regions according to the distance  $r_{n_e}$  of the scattering electron, i.e., photoelectron, and the center of mass of the molecular ion having  $(n_e - 1)$  electrons. In the inner region, defined by condition  $r_{n_e} < a$ , the  $n_e$ -electron wave functions of the total system are represented by  $(n_e - 1)$ -electron wave functions of molecular ion augmented by diffuse functions which describe a scattering electron,

$$\Phi_k = \mathcal{A} \sum_{ij} \bar{\phi}_i(x_1, \dots, x_{n_e-1}, \sigma_{n_e}) u_j(\mathbf{r}_{n_e}) a_{ij} + \sum_q X_q(x_1 \dots x_{n_e}) b_q, \quad (7)$$

where  $\mathcal{A}$  is an antisymmetrization operator,  $x_i$  represents spacial and spin coordinates of the  $i$ th electron,  $\bar{\phi}_i$  are the eigenstate of the total spin and its z component constructed from the  $(n_e - 1)$ -electron wave functions of the molecular ion  $\phi_i$  and the spin function of the scattering electron,  $u_j$  are continuum orbitals representing wave functions of the scattering electron, and  $X_q$  are bound  $n_e$  electron wave functions composed of the target molecular orbitals and the extra target virtual orbitals, the coefficients  $a_{ij}$  and  $b_q$  are determined by diagonalization of  $H_{n_e} + L_{n_e}$  where  $H_{n_e}$  is the electronic Hamiltonian and  $L_{n_e}$  is a Bloch operator<sup>28,29</sup> accounting for surface term. In the outer region  $r_{n_e} > a$ , the problem is reduced to single electron scattering, ignoring exchange of the scattering electron with the electrons of the molecular ion. Interaction of the scattering electron and the molecular ion is considered through static multipolar interaction potentials which introduce inter-channel couplings. The R-matrix eigenstates obtained by diagonalization of the Hamiltonian in the inner region are converted to the R-matrix  $R_{ij}$  at the boundary  $r_{n_e} = a$  as,

$$R_{ij}(E) = \frac{1}{2a} \sum_k \frac{w_{ik}(a) w_{jk}(a)}{E_k - E}, \quad (8)$$

where  $E_k$  is eigenvalue of  $\Phi_k$ ,  $E$  is the energy of the total system, and the boundary amplitudes  $w_{ik}$  is given by

$$w_{ik}(r) = \langle \bar{\phi}_i Y_{l_i m_i} | \Phi_k \rangle. \quad (9)$$

For photoionization problem, the final states  $\Psi_{l_f m_f}^{f-}$  in Eq. (3) are expanded by the R-matrix eigenstates  $\Phi_k$  as<sup>18</sup>,

$$\Psi_f^- = \sum_k A_{kf} \Phi_k. \quad (10)$$

Here  $\Psi_{l_f m_f}^{f-}$  is denoted as  $\Psi_f^-$  for simplicity. Using the relation<sup>18,30</sup> which holds for the R-matrix amplitudes and the final state wave functions, the expansion coefficients can be

written as,

$$A_{kf} = \frac{1}{2a(E_k - E_f)} \sum_j w_{jk}(a) \left( a \frac{dy_{jf}}{dr} - by_{jf} \right)_{r=a}, \quad (11)$$

where  $E_f$  is the energy of the final state, which is equal to  $E_i + E_r$  with the initial state energy  $E_i$  and the photon energy  $E_r$ . The parameter  $b$  is related to the logarithmic derivative of the scattering electron wavefunction at the R-matrix boundary and is set to zero in this work. The radial function  $y_{jf}$  is defined as

$$y_{jf} = \langle \bar{\phi}_j Y_{l_j m_j} | \Psi_f^- \rangle. \quad (12)$$

We have to determine the radial functions and their derivatives in Eq. (11) to evaluate the final state wave functions. In the outer region, the radial functions  $y_{jf}$  satisfy the differential equations<sup>18,30</sup>,

$$\left( \frac{d^2}{dr^2} - \frac{l_i(l_i + 1)}{r^2} + \frac{2z}{r} + k_j^2 \right) y_j(r) = 2 \sum_{k=1}^n V_{jk}(r) y_k(r), \quad (13)$$

where  $n$  is the number of channels considered in the R-matrix model,  $z$  is the net charge of the molecular ion,  $k_j$  is the wavenumber of the electron in the  $j$ th channel and  $V_{jk}(r)$  represents multipole potential.<sup>30</sup> When  $n_a$  channels are open, we have  $n + n_a$  independent solutions of Eq. (13) with the asymptotic boundary conditions,

$$\begin{aligned} v_{ij}(r) &\underset{r \rightarrow \infty}{\sim} k_i^{-1/2} \sin \theta_i \delta_{ij} & i = 1, \dots, n, \quad j = 1, \dots, n_a \\ v_{ij}(r) &\underset{r \rightarrow \infty}{\sim} k_i^{-1/2} \cos \theta_i \delta_{ij-n_a} & i = 1, \dots, n, \quad j = n_a + 1, \dots, 2n_a \\ v_{ij}(r) &\underset{r \rightarrow \infty}{\sim} \exp(-|k_i|r) \delta_{ij-n_a} & i = 1, \dots, n, \quad j = 2n_a + 1, \dots, n + n_a \end{aligned} \quad (14)$$

where

$$\theta_i = k_i r - \frac{1}{2} l_i \pi - \eta_i \ln(2k_i r) + \arg \Gamma(l_i + 1 + i\eta_i) \quad i = 1, \dots, n_a \quad (15)$$

with  $\eta_i = -z/k_i$ . The radial functions  $y_{jf}$  are expanded by these  $n+n_a$  independent solutions  $v_{ij}$  as,

$$y_{jf} = \sum_{k=1}^{n+n_a} v_{jk} x_k. \quad (16)$$

By inserting Eq. (16) into the R-matrix relation<sup>18,30</sup>,

$$y_{jf}(a) = \sum_{k=1}^n R_{jk} \left( a \frac{dy_{kf}}{dr} - by_{kf} \right) \quad j = 1, \dots, n, \quad (17)$$

and using the ingoing wave asymptotic conditions of  $y_f$ ,

$$[y_f^-]_{ij} \underset{r \rightarrow \infty}{\sim} \sum_{k=1}^{n_a} k_i^{-1/2} (\sin \theta_i \delta_{ik} + \cos \theta_i K_{ik}) [(\mathbf{1} + i\mathbf{K})^{-1}]_{kj} \quad i, j = 1, \dots, n_a, \quad (18)$$

with  $\mathbf{K}$  and  $K_{ik}$  being K-matrix and its elements, we obtain  $(n + n_a)$  linear equations for  $(n + n_a)$  unknown coefficients  $x_k$ . The expansion coefficients  $x_k$  can be determined by solving these equations, and as a result, we can evaluate the final state wavefunctions  $\Phi_f^-$  using Eqs. (10) and (11).

In this work, the initial state wave function  $\Psi_i$  is also expanded by the R-matrix eigenstates as described in Burke and Taylor<sup>18</sup>,

$$\Psi_i = \sum_k A_{ki} \Phi_k, \quad (19)$$

where the coefficient  $A_{ki}$  is given by Eq. (11) with  $E_f$  and  $y_{jf}$  replaced by the energy  $E_i$  and the radial function  $y_{ji}$  of the initial state. The radial functions  $y_{ji}$  are expanded by the independent solutions of the differential equations (13) as,

$$y_{ji} = \sum_{k=1}^n v_{jk} x_k. \quad (20)$$

Since we are treating bound initial state, all channels are closed,  $n_a = 0$ , and all independent solutions decay to zero as  $r$  approaches infinity. By substituting Eq. (20) into the R-matrix relation of Eq. (17),  $n$  equations for  $n$  unknown coefficients  $x_k$  are obtained. These equations are only solved at discrete energies of  $E_i$ , where the lowest of them corresponds to the ground state energy of the neutral molecule.

### III. APPLICATION OF THE METHOD TO PHOTOIONIZATION OF N<sub>2</sub> AND NO MOLECULES

#### A. Detail of the calculations

Cross sections and asymmetry parameters for valence electron photoionization of N<sub>2</sub> and NO molecules were calculated based on the method described in the previous section. The R-matrix eigenstates and amplitudes were obtained by electron - N<sub>2</sub><sup>+</sup> and NO<sup>+</sup> scattering calculations using a modified version of the polyatomic programs in the UK molecular R-matrix codes<sup>13</sup>. We used the fixed nuclei approximation with internuclear distances 2.068 a<sub>0</sub>

for  $\text{N}_2$  and  $2.175 a_0$  for  $\text{NO}$ , which are the equilibrium values of the ground electronic states of  $\text{N}_2$  and  $\text{NO}$ .

For the electron -  $\text{N}_2^+$  R-matrix scattering calculation, we employed two R-matrix models; a single-channel SCF target model and a multi-channel CI target model including 80  $\text{N}_2^+$  electronic states. The cc-pVTZ atomic basis set<sup>31</sup> was used to describe molecular orbitals in both models. In the CI target model, full valence complete active space was employed to generate configuration state functions for the  $\text{N}_2^+$  electronic states. The molecular orbitals (MOs) in this active space were obtained by the state-averaged complete active space self consistent field (CASSCF)<sup>32,33</sup> calculation using molpro program package<sup>34</sup>. The state-averaging was performed over the lower 28 electronic states of  $\text{N}_2^+$  ion, then the CASCI wave functions of the remaining 52 electronic states were constructed from this CASSCF molecular orbital set. The CASSCF ionization potentials of the lower 9  $\text{N}_2^+$  electronic states are listed in Table I, where the  $\text{N}_2$  ground state energy was obtained by the electron -  $\text{N}_2^+$  scattering calculation, as described at the end of the last section. In addition to these CASSCF MOs for the  $\text{N}_2^+$  valence electronic states, we included 3 extra virtual orbitals for each irreducible representation of the  $D_{2h}$  symmetry. In order to represent the scattering electron, we included diffuse Gaussian functions up to  $l = 5$ , with 12 functions for  $l = 0$  and 1, 8 functions for  $l = 2$  and 3, and 5 functions for  $l = 4$  and 5. Exponents of these diffuse Gaussians were obtained by the GTOBAS program<sup>35</sup> in the UK R-matrix codes. To prepare an orthogonal MO set used in Eq. (7), these Gaussian functions were orthogonalized against the valence and extra virtual MOs obtained by the CASSCF calculation. The procedure for construction of the 14-electron configurations in Eq. (7) is almost the same as we did in the previous work of electron -  $\text{N}_2$  scattering calculation<sup>24</sup>, except the number of electron in the system, and is not repeated here. Radius of the R-matrix sphere was chosen to be  $10 a_0$  in our calculations. The R-matrix calculations were performed for the singlet  $A_g$ ,  $B_{1u}$ ,  $B_{2u}$  and  $B_{3u}$  symmetries of the  $e+\text{N}_2^+$  system, where the  $A_g$  result was used for the ground state of the neutral molecule whereas the other symmetries were used to construct the final state wavefunctions.

Detail of the electron -  $\text{NO}^+$  R-matrix scattering calculation is similar to the electron -  $\text{N}_2^+$  scatterings. In this case, we performed a single-channel SCF target calculation and a multi-channel CI target calculation with 60  $\text{NO}^+$  electronic states. The state-averaged CASSCF calculation with cc-pVTZ basis set was performed for the lowest 16 electronic



states of  $\text{NO}^+$ , then the CASCI wave functions were constructed for the other states. The ionization potentials of the lowest 8  $\text{NO}^+$  electronic states are shown in Table II. Radius of the R-matrix sphere and diffuse Gaussian functions for the scattering electron are the same as in the  $e\text{-N}_2^+$  calculation. In this  $e\text{-NO}^+$  calculation, we included 4 extra virtual orbitals for each irreducible representation of the  $C_{2v}$  symmetry. The R-matrix calculations were performed for the doublet  $A_1$ ,  $A_2$  and  $B_1$  symmetries of the  $e+\text{NO}^+$  system, where the  $B_1$  result was used to describe both the ground state of the neutral molecule and the final state wavefunctions, whereas the other symmetries were only used for the final states.

The wave functions of the initial  $\text{N}_2X^1\Sigma_g^+$  and  $\text{NOX}^2\Pi$  states were expanded by the R-matrix eigenstates taken from the  $e\text{-N}_2^+$  and  $e\text{-NO}^+$  R-matrix scattering calculations as described at the end of the last section, and their expansion coefficients were obtained by the BOUND module of the UK R-matrix codes. It was found that the wave functions of these  $\text{N}_2$  and  $\text{NO}$  states are dominated by the lowest eigenvalue R-matrix eigenstates, i.e., expansion coefficients of the lowest eigenvalue states are almost unity whereas they are less than  $10^{-4}$  for the other R-matrix eigenstates. Thus, we just substituted the initial state wave functions in Eq. (3) by these lowest eigenvalue R-matrix eigenstates. Note that the above procedure means that the ground state wavefunction of the neutral molecule is described by the MOs of the molecular ion. This is approximate method for description of the ground state wavefunctions, however, it greatly simplifies evaluation of the transition dipole moments, since the same set of MOs is used in the initial and the final state wavefunctions.

In order to obtain the transition dipole matrix elements of Eq. (3), we evaluated the dipole matrix elements between the R-matrix eigenstates. Then the expansion coefficients for the final state wave functions were calculated using Eqs. (11) and (16). In principle, accurate solutions of differential equations (13) with proper boundary conditions (14) have to be used for Eq. (16). Such solutions are usually prepared by the asymptotic expansion<sup>36,37</sup> and inward integration to the matching point  $r = a$ . However, the asymptotic expansion is not so accurate for small  $r$  and near the ionization thresholds, where we have 80 such thresholds for  $\text{N}_2$  photoionization and 60 for  $\text{NO}$  molecule in our R-matrix models. Also, inward integration is unstable due to exponential growing of closed channel components. In this work, we approximated  $v_{ij}$  by the Coulomb functions ignoring multipole potentials of the molecular ions. Based on the calculated transition dipole moments, photoionization cross sections and asymmetry parameters were evaluated using Eqs. (2), (5) and (6).

## B. Results and Discussion

### 1. Ionization Potentials

In Table I, the CASSCF ionization energies of  $N_2$  molecule are shown for the lower  $N_2^+$  ion states with the experimental values<sup>38</sup>. Our results agree reasonably well with the experimental ionization energies, though ours are 0.5 - 1.0 eV higher. The ionization potentials of NO molecule are also shown for the lowest 8  $NO^+$  ion states in Table II. Since the equilibrium bond distances of some excited states are longer than that of the neutral NO ground state<sup>39</sup>, energetic order of the  $A^1\Pi$ ,  $A'^1\Sigma^-$  and  $W^1\Delta$  states in our results is different from that in the adiabatic experimental results. Nevertheless, our IPs compare reasonably well with the experiment, with deviations less than 1 eV. Note that the IPs in Tables I and II were extracted from the ionic and neutral energies used in the R-matrix photoionization calculations. Since we did not attempt to adjust these energies to the experimental IPs, the ionization thresholds in our cross sections and asymmetry parameters are shifted relative to the correct experimental values.

### 2. $N_2$

In Fig. 1, cross section and asymmetry parameter for photoionization of the  $N_2X^1\Sigma_g^+$  state leading to the  $N_2^+X^2\Sigma_g^+$  state are shown. In the figure, our CASSCF results and SCF results are compared with the previous theoretical results of Montuoro and Moccia<sup>6</sup> obtained by the K-matrix method with interacting channels random phase approximation and Stratmann et al.<sup>40</sup> obtained by the multi-channel Schwinger variational method. Also, the experimental cross sections of Hamnett et al.<sup>41</sup>, Samson et al.<sup>42</sup>, Plummer et al.<sup>43</sup>, and the asymmetry parameters of Marr et al.<sup>44</sup> and Southworth et al.<sup>45</sup> are included in the figure. Our SCF cross section is smooth and has a large broad peak around 30 eV, originated from the  $\sigma^*$  shape resonance. In contrast, our CASSCF multi-channel cross section has numerous sharp peaks originated from two- or many-electron excited resonances as well as Rydberg resonances associated with the excited electronic states of  $N_2^+$  ion. Overall shape of the cross section is roughly similar to the SCF result. The CASSCF cross section rises at low energy region around 15-20 eV, which is consistent with the experimental result of Hamnett et al. and Samson et al. and the previous theoretical cross section of Montuoro and Moccia. Below

30 eV, our CASSCF cross section agrees well, except for the presence of the sharp peaks, with the experimental results. However, it overestimates the experimental values above 30 eV. The SCF cross section agrees rather well with the experimental results in this high energy region. Similar to the calculated cross sections, the CASSCF asymmetry parameter  $\beta$  has numerous sharp peaks while the SCF asymmetry parameter is very smooth. Compared to the SCF result, the CASSCF result agrees better with the experimental asymmetry parameters in all energy range in the figure. At low energy region below 24 eV, the CASSCF R-matrix calculation overestimates the experimental asymmetry parameters, partly due to existence of resonances. The cross section and asymmetry parameter of Stratmann et al. are available over limited energy range of 19 - 26 eV. In this energy region, our CASSCF results are very similar to their results.

Figure 2 shows photoionization cross section and asymmetry parameter for the  $N_2^+ A^2\Pi$  state, where our CASSCF results are compared with the previous theoretical results of Stratmann et al.<sup>40</sup> and the experimental cross sections of Hamnett et al.<sup>41</sup>, Samson et al.<sup>42</sup>, Plummer et al.<sup>43</sup>, and the experimental asymmetry parameter of Marr et al.<sup>44</sup> Shape of our CASSCF cross section is roughly similar to the experimental results. However, magnitude of our cross section is slightly larger than the experimental cross sections above 25 eV. In case of the asymmetry parameter, our result agrees very well, except for the presence of the small peaks, with the experimental result of Marr et al. The previous multi-channel Schwinger results of Stratmann et al. are available between 19 and 26 eV. In this energy region, the shape of our cross section is very similar to their result, although magnitude of cross section is larger than theirs. For the asymmetry parameter, our result almost coincides with the result of Stratmann et al.

In Fig. 3, cross section and asymmetry parameter for photoionization leading to the  $N_2^+ B^2\Sigma_u^+$  state are shown with the available experimental results and the previous theoretical results of Stratmann et al.<sup>40</sup> As in the photoionization to the  $N_2^+ A^2\Pi$  state, our cross section is slightly larger than the result of Stratmann et al., however, the asymmetry parameter is very similar to each other. Compared to the experimental results, our cross section looks larger near the threshold, yet, agreement is better at higher energies. On average, our asymmetry parameter is roughly similar to the experimental results, however, the experimental asymmetry parameter has a large dip around 30 eV which does not exist in our results. In the previous studies<sup>6,45</sup>, a coupling between the  $X^2\Sigma_g^+$  and  $B^2\Sigma_u^+$  channels

has been suggested to cause this large dip. Although such a coupling is included in our model, our asymmetry parameter is rather flat between 20 and 45 eV, with slight decrease of magnitude around 35 eV.

In general, partial photoionization cross sections for the higher  $N_2^+$  ion states are very small compared to those for the  $N_2^+ X^2\Sigma_g^+$ ,  $A^2\Pi$  and  $B^2\Sigma_u^+$  states. However, the photoionization cross section leading to the  $2^2\Sigma_g^+$  state is relatively large. The calculated cross section and asymmetry parameter are shown in Fig. 4. The ionization energy of this  $N_2^+ 2^2\Sigma_g^+$  state is about 29.65 eV, which is close to the threshold of the “Z” state mentioned in Hamnett et al.<sup>41</sup> Their cross section for the “Z” state is also shown in Fig. 4. Although agreement is not so good, the magnitudes of the cross sections are roughly similar to each other. The calculated asymmetry parameter drops from 1.5 at the threshold to -0.5 near 35 eV, then it increases to 0.5 at 45 eV. This behaviour differs from the asymmetry parameters for the  $N_2^+ X$ ,  $A$  and  $B$  states, probably reflecting the difference in the main electronic configurations of the ionic states.

### 3. NO

In Fig. 5, cross section and asymmetry parameter for photoionization of the  $NOX^2\Pi$  leading to the  $NO^+ X^1\Sigma^+$  state are shown with the experimental results of Southworth et al.<sup>46</sup> and Iida et al.<sup>47</sup>, and the previous theoretical results of Stratmann et al.<sup>25</sup> Our CASSCF cross section has numerous sharp peaks between 13 and 18 eV, mostly originated from Rydberg resonances associated with the excited electronic states of  $NO^+$ . In the other energy region, the magnitude of the cross section is nearly constant value of about 5 Mb. Compared to the CASSCF result, the SCF cross section is very smooth and flat. Although a slight increase of the SCF cross section exists around 16 eV, the height of the peak is much smaller than the CASSCF cross section around this energy region. The shape of our CASSCF cross section is very similar to the result of Stratmann et al, especially above 14 eV. Between 12.5 and 14eV, our cross section has several sharp peaks as in the higher energy region. In contrast, there is no such peak in the cross section of Stratmann et al. below 14 eV. Below 25 eV, our CASSCF cross section agrees well, except for the presence of the sharp peaks, with the experimental cross section of Southworth et al. Our result, however, slightly underestimates experimental cross section above 25 eV. Compared to the result of

Iida et al, the magnitude of our CASSCF cross section is generally smaller except in the high energy region around 35-40 eV. Enhancement of cross section is observed below 20 eV in the experimental results of Southworth et al. and Iida et al., which is roughly reproduced by our CASSCF R-matrix calculation. However, this feature is not well captured in the SCF R-matrix model. The shape of our CASSCF asymmetry parameter is roughly similar to the result of Stratmann et al. The asymmetry parameter of Stratmann et al. is rather steeper above 18eV, and agrees better with the experimental result of Southworth et al. Our SCF asymmetry parameter has a much smoother profile compared to the CASSCF result. Its tilt is close to the results of Stratmann et al. and Southworth et al., though the magnitude is generally larger.

Figure 6 shows cross section and asymmetry parameter for ionization to the  $\text{NO}^+b^3\Pi$  state. The experimental results of Southworth et al.<sup>46</sup> are also included in the figure. Near the ionization threshold, our cross section has many peaks as in the cross section of the  $\text{NO}^+X^1\Sigma^+$  state. The magnitude of the cross section increases from 5 Mb to 7 Mb as photon energy increases from the threshold to 27 eV. Then it decreases to about 3 Mb at 40 eV. Although overall shape of the cross section is similar to the experimental result, the broad peak in our result is located 3-4 eV higher in energy compared to the peak in the experimental cross section. Our asymmetry parameter decreases from 1.5 to 0.4 as energy increases from the threshold to 40 eV. This behaviour is roughly similar to the experimental result, however, our asymmetry parameter has a dip around 20-25 eV whereas there is a small bump in this energy region in the experimental result.

In Fig. 7, cross section and asymmetry parameter for photoionization to the  $\text{NO}^+A^1\Pi$  state are shown with the previous theoretical results of Stratmann et al.<sup>25</sup> Our cross section is generally larger than their result above 22 eV. The shapes of the cross sections resemble each other, having a broad peak around 25 eV. The asymmetry parameter gradually decreases from 1.5 at the threshold to 0.15 at 40 eV. Our result has a dip around 23 eV which does not exist in the asymmetry parameter of Stratmann et al., however, the other details are similar.

In Fig. 8, photoionization cross sections and asymmetry parameters for the  $\text{NO}^+w^3\Delta$ ,  $a^3\Sigma^+$ ,  $A'^1\Sigma^-$ ,  $b'^3\Sigma^-$  and  $W^1\Delta$  states are shown with the averaged experimental asymmetry parameter of Southworth et al.<sup>46</sup> The cross sections for the  $a$ ,  $A'$ ,  $b'$  and  $W$  states are relatively flat above the thresholds and are similar to each other. The cross section for the

$w$  state decreases slowly from the threshold to 40 eV, with a drop around 20-23 eV. The magnitude of cross section is the largest for the  $w^3\Delta$  state with average value of about 5 Mb. The magnitude of the cross sections for the  $a^3\Sigma^+$ ,  $b^3\Sigma^-$  and  $W^1\Delta$  states is about 2.0-2.5 Mb, and the  $A'^1\Sigma^-$  state has the smallest magnitude of about 1.0 Mb. The asymmetry parameters of these states have remarkably similar shapes and magnitudes, starting from -0.8 at the thresholds and increasing monotonically to 1.2 around 40 eV. Our results agree well with the experimental averaged asymmetry parameter of Southworth et al.

#### 4. Discussion

The photoionization cross sections and asymmetry parameters calculated in this work have numerous sharp narrow peaks. They are originated from the Rydberg resonances associated with the excited electronic states of the molecular ions as well as two- or many-electron excited resonances. This can be checked by changing number of excited ionic states included in the R-matrix calculation or by modification of the  $X_q$  terms in Eq. (7). These sharp resonances are characteristic of multi-channel method such as present CASSCF multi-channel R-matrix calculation and the Schwinger multi-channel method. Since they are not described in the single-channel SCF target R-matrix calculation, the SCF cross section and asymmetry parameter in Figs 1 and 5 are very smooth. These numerous peaks are rarely seen in the previous theoretical calculations because many of them used single-channel method. The cross sections and asymmetry parameters of Stratmann et al.<sup>25</sup>, calculated by the Schwinger multi-channel method, are very similar to our CASSCF results, including location of several peaks. For NO photoionization, some energy regions exist where our results have many narrow peaks whereas the results of Stratmann et al. are smooth. This discrepancy is attributed to difference of  $\text{NO}^+$  electronic states included in the calculations. For example, Stratmann et al. did not include  $\text{NO}^+$  ionic states with  $(\pi)^{-1}$  configuration, however, we put these electronic states in the R-matrix model. These narrow peaks in our results are not observed in the previous experimental results. In this work, we employed the fixed nuclei approximation. However, if we include the effect of vibrational motion by using the adiabatic averaging method or the non-adiabatic R-matrix method, these narrow sharp peaks may be averaged and look less prominent.

As can be seen from the figures, the shapes of the photoionization asymmetry parameters

are closely related to the main electronic configuration of the molecular ion, in other words, the molecular orbital from which ionization occurs. When the molecular ion has a  $(\sigma)^{-1}$  configuration, e.g.,  $N_2^+ X^2\Sigma_g^+$  and  $NO^+ b^3\Pi$  states, the asymmetry parameter is generally 0.5-1.0 near the threshold and remains nearly constant or decreases slightly with energy. In contrast, when the configuration is  $(\pi)^{-1}$  type, e.g.,  $N_2^+ A^2\Pi_u$  and  $NO^+ X^1\Sigma^+$  states, the asymmetry parameter is negative or zero near the threshold and increases rapidly with photon energy. These behaviour have been discussed by several authors including Southworth et al.<sup>46</sup> and Thiel<sup>48</sup>, and are interpreted in terms of angular momentum components of photoelectrons near threshold.

In our model, angular momentum of photoelectron was considered up to  $l = 5$ . Photoionization cross sections and asymmetry parameters obtained by maximum angular momentum of  $l = 3$  and 5 are very similar to each other, which suggests that we do not have to increase  $l$  more than 5 in this study. Concerning number of excited electronic states of molecular ion, we included 80 and 60 electronic states of  $N_2^+$  and  $NO^+$  ions, respectively. This inclusion of many excited ionic states is necessary to obtain converged cross sections and asymmetry parameters as well as to suppress pseudo resonances. The numbers of states in our models are much larger than those in the previous Schwinger multi-channel calculations of Stratmann et al.<sup>25,40</sup> In the asymptotic region, we considered only the Coulomb potential in this work. In order to inspect the effect of dipole and quadrupole potentials on resonance position, we calculated elastic cross sections of electron -  $N_2^+$  and  $NO^+$  collisions with and without the multipole potentials, using CASSCF multi-channel R-matrix models. As in the photoionization cross sections shown in the figures, the elastic cross sections of the electron-ion collisions contain many sharp resonance peaks. As far as we have checked, the effect of the multipole potentials on resonance position in these elastic cross sections is not significant, less than 0.01 eV. This observation suggests that arrangement of resonances in photoionization cross section does not change much by introduction of the multipole potentials, at least for  $N_2$  and  $NO$  molecules. However, when accurate assignment of Rydberg resonances and determination of quantum defects are of interest, consideration of dipole and quadrupole potentials will be important.

In this work, we used the SA-CASSCF MOs of the molecular ion,  $N_2^+$  or  $NO^+$ , to describe the ground electronic state of the neutral molecule,  $N_2 X^2\Sigma_g^+$  or  $NO X^2\Pi$ . Using a single set of MOs for both the initial and final states makes evaluation of transition dipole matrix

elements much easier and faster than using non-orthogonal MO sets optimized for neutral and ionic electronic states separately. Our SA-CASSCF MOs are not optimized for neutral molecule, thus, the full-valence CASCI energy of the neutral molecule obtained by these ionic MOs is generally higher than the energy obtained by neutral MOs. Since we have extracted the energy of the neutral molecule by the R-matrix scattering calculation, the ground state wavefunction of the neutral molecule is constructed from the configuration with the valence MOs as well as the additional configurations which contain diffuse orbitals, as described by Burke and Taylor<sup>18</sup> and explained at the end of the last section. Inclusion of these additional configurations generally lowers the ground state energy compared to the full-valence CASCI energy. For valence electron photoionization, the effects of these ionic MOs and the additional configurations appear to compensate each other, since deviations of the calculated IPs from the experimental values are not significant as shown in Table I and II. However, in case of inner-shell ionization, this compensation does not work well, e.g., the ionization threshold for the  $N_2^+(1\sigma_g)^{-1}$  state is about 4 eV lower than the experimental value in our preliminary calculation. Thus, we may need to use non-orthogonal MO sets to describe neutral and ionic states, when the R-matrix method is applied to inner-shell photoionization.

Comparison of our calculation with the previous experimental and theoretical works demonstrates that the R-matrix method is well suited to treat valence electron photoionization of closed-shell as well as open-shell molecules such as  $N_2$  and  $NO$ . We implemented the method as simple as possible. So, effects of the velocity form dipole moment, multipole potentials, vibrational motion etc. are not discussed or considered in this paper. In the future, we will study these issues along with application of the method to inner-shell molecular photoionization.

#### IV. SUMMARY

In this work, we implemented the R-matrix method to treat molecular photoionization based on the procedure described by Burke and Taylor<sup>18</sup>. For the inner region calculation, the polyatomic version of the UK R-matrix codes was used with some modifications. Final state wavefunctions of molecular photoionization were represented by linear combinations of the R-matrix eigenstates obtained by diagonalization of the electronic Hamiltonian inside



the inner region. Then, transition dipole matrix elements between the initial and the final states were calculated for evaluation of observables such as photoionization cross section and asymmetry parameter. As test calculations, we applied this method to valence electron photoionization of  $\text{N}_2$  and  $\text{NO}$  molecules. In our R-matrix models, the electronic states of the molecular ions,  $\text{N}_2^+$  and  $\text{NO}^+$ , were represented by full-valence complete active space CI wavefunctions with cc-pVTZ basis set. Calculated photoionization cross sections and asymmetry parameters have many narrow peaks originated from two- or many-electron excited resonances as well as Rydberg resonances associated with the excited electronic states of  $\text{N}_2^+$  or  $\text{NO}^+$ , which are very similar to the previous theoretical results of Stratmann et al.<sup>25,40</sup> obtained by the multi-channel Schwinger calculations. Overall shapes of the calculated cross sections and asymmetry parameters agree reasonably well, except for the presence of the sharp peaks, with the available experimental results.

## ACKNOWLEDGMENTS

The author wishes to acknowledge the helpful comments of Professors Keiji Morokuma and Shigeki Kato.

## REFERENCES

- <sup>1</sup>T. Suzuki, *Annu. Rev. Phys. Chem.* **57**, 555 (2006).
- <sup>2</sup>K. L. Reid, *Annu. Rev. Phys. Chem.* **54**, 397 (2003).
- <sup>3</sup>K. Ueda, *J. Phys. B* **36**, R1 (2003).
- <sup>4</sup>R. R. Lucchese, K. Takatsuka, and V. McKoy, *Phys. Rep.* **131**, 147 (1986).
- <sup>5</sup>S. K. Semenov and N. A. Cherepkov, *Chem. Phys. Lett.* **291**, 375 (1998).
- <sup>6</sup>R. Montuoro and R. Moccia, *Chem. Phys.* **293**, 281 (2003).
- <sup>7</sup>M. Stener, D. Toffoli, G. Fronzoni, and P. Decleva, *Theor. Chem. Acc.* **117**, 943 (2007).
- <sup>8</sup>T. N. Rescigno and C. W. McCurdy, *Phys. Rev. A* **31**, 624 (1985).
- <sup>9</sup>T. Yasuike and S. Yabushita, *Chem. Phys. Lett.* **316**, 257 (2000).
- <sup>10</sup>P. Langhoff, *Chem. Phys. Lett.* **22**, 60 (1973).
- <sup>11</sup>E. P. Wigner and L. Eisenbud, *Phys. Rev.* **72**, 29 (1947).
- <sup>12</sup>K. A. Berrington, W. B. Eissner, and P. H. Norrington, *Comput. Phys. Commun.* **92**, 290 (1995).
- <sup>13</sup>L. A. Morgan, J. Tennyson, and C. J. Gillan, *Comput. Phys. Commun.* **114**, 120 (1998).
- <sup>14</sup>J. Tennyson and L. A. Morgan, *Philos. T. Roy. Soc. A* **357**, 1161 (1999).
- <sup>15</sup>J. D. Gorfinkiel, A. Faure, S. Taioli, C. Piccarreta, G. Halmova, and J. Tennyson, *Eur. Phys. J. D* **35**, 231 (2005).
- <sup>16</sup>P. G. Burke and J. Tennyson, *Mol. Phys.* **103**, 2537 (2005).
- <sup>17</sup>T. N. Rescigno, B. H. Lengsfeld, and A. E. Orel, *J. Chem. Phys.* **99**, 5097 (1993).
- <sup>18</sup>P. G. Burke and K. T. Taylor, *J. Phys. B* **8**, 2620 (1975).
- <sup>19</sup>P. G. Burke, P. Francken, and C. J. Joachain, *J. Phys. B* **24**, 761 (1991).
- <sup>20</sup>P. G. Burke, J. Colgan, D. H. Glass, and K. Higgins, *J. Phys. B* **33**, 143 (2000).
- <sup>21</sup>J. Tennyson, C. J. Noble, and P. G. Burke, *Int. J. Quantum Chem.* **29**, 1033 (1986).
- <sup>22</sup>J. Colgan, D. H. Glass, K. Higgins, and P. G. Burke, *J. Phys. B* **34**, 2089 (2001).
- <sup>23</sup>M. Tashiro, K. Morokuma, and J. Tennyson, *Phys. Rev. A* **74**, 022706 (2006).
- <sup>24</sup>M. Tashiro and K. Morokuma, *Phys. Rev. A* **75**, 012720 (2007).
- <sup>25</sup>R. E. Stratmann, R. W. Zures, and R. R. Lucchese, *J. Chem. Phys.* **104**, 8989 (1996).
- <sup>26</sup>N. Chandra, *Chem. Phys.* **108**, 301 (1986).
- <sup>27</sup>N. Chandra, *J. Phys. B* **20**, 3405 (1987).
- <sup>28</sup>C. Bloch, *Nucl. Phys.* **4**, 503 (1957).

- <sup>29</sup>K. Pfingst, B. M. Nestmann, and S. D. Peyerimhoff, *J. Phys. B* **27**, 2283 (1994).
- <sup>30</sup>P. G. Burke, A. Hibbert, and W. D. Robb, *J. Phys. B* **4**, 153 (1971).
- <sup>31</sup>T. H. Dunning, Jr., *J. Chem. Phys.* **90**, 1007 (1989).
- <sup>32</sup>P. J. Knowles and H.-J. Werner, *Chem. Phys. Lett.* **115**, 259 (1985).
- <sup>33</sup>H.-J. Werner and P. J. Knowles, *J. Chem. Phys.* **82**, 5053 (1985).
- <sup>34</sup>MOLPRO version 2008.3, a package of ab initio programs written by H.-J. Werner, P. J. Knowles, R. Lindh, F. R. Manby, M. Schütz, P. Celani, T. Korona, A. Mitrushenkov, G. Rauhut, T. B. Adler, R. D. Amos, A. Bernhardsson, A. Berning, D. L. Cooper, M. J. O. Deegan, A. J. Dobbyn, F. Eckert, E. Goll, C. Hampel, G. Hetzer, T. Hrenar, G. Knizia, C. Köppl, Y. Liu, A. W. Lloyd, R. A. Mata, A. J. May, S. J. McNicholas, W. Meyer, M. E. Mura, A. Nicklass, P. Palmieri, K. Pflüger, R. Pitzer, M. Reiher, U. Schumann, H. Stoll, A. J. Stone, R. Tarroni, T. Thorsteinsson, M. Wang, and A. Wolf.
- <sup>35</sup>A. Faure, J. D. Gorfinkiel, L. A. Morgan, and J. Tennyson, *Comput. Phys. Commun.* **144**, 224 (2002).
- <sup>36</sup>P. G. Burke and H. M. Schey, *Phys. Rev.* **126**, 147 (1962).
- <sup>37</sup>M. Gailitis, *J. Phys. B* **9**, 843 (1976).
- <sup>38</sup>P. Baltzer, M. Larsson, L. Karlsson, B. Wannberg, and M. C. Gothe, *Phys. Rev. A* **46**, 5545 (1992).
- <sup>39</sup>D. L. Albritton, A. L. Schmeltekopf, and R. N. Zare, *J. Chem. Phys.* **71**, 3271 (1979).
- <sup>40</sup>R. E. Stratmann, G. Bandarage, and R. R. Lucchese, *Phys. Rev. A* **51**, 3756 (1995).
- <sup>41</sup>A. Hamnett, W. Stoll, and C. E. Brion, *J. Electron Spectrosc. Relat. Phenom.* **8**, 367 (1976).
- <sup>42</sup>J. A. R. Samson, G. N. Haddad, and J. L. Gardner, *J. Phys. B* **10**, 1749 (1977).
- <sup>43</sup>E. W. Plummer, T. Gustafsson, W. Gudat, and D. E. Eastman, *Phys. Rev. A* **15**, 2339 (1977).
- <sup>44</sup>G. V. Marr, J. M. Morton, R. M. Holmes, and D. G. McCoy, *J. Phys. B* **12**, 43 (1979).
- <sup>45</sup>S. H. Southworth, A. C. Parr, J. E. Hardis, and J. L. Dehmer, *Phys. Rev. A* **33**, 1020 (1986).
- <sup>46</sup>S. Southworth, C. M. Truesdale, P. H. Kobrin, D. W. Lindle, W. D. Brewer, and D. A. Shirley, *J. Chem. Phys.* **76**, 143 (1982).
- <sup>47</sup>Y. Iida, F. Carnovale, S. Daviel, and C. E. Brion, *Chem. Phys.* **105**, 211 (1986).
- <sup>48</sup>W. Thiel, *Chem. Phys.* **77**, 103 (1983).

## LIST OF FIGURES

1	Photoionization cross section (a) and asymmetry parameter (b) for ionization of the $N_2^+ X^2\Sigma_g^+$ state. The cross sections are shown in unit of mega barn (Mb), equal to $10^{-22}m^2$ . Our CASSCF target results and SCF target results are represented as thick full lines and thick dashed lines, respectively. The previous theoretical results of Montuoro and Moccia <sup>6</sup> and Stratmann et al. <sup>40</sup> are shown as thin dotted and thin dashed lines, respectively. Experimental data included in the panel (a) are taken from Hamnett et al. <sup>41</sup> , Samson et al. <sup>42</sup> and Plummer et al. <sup>43</sup> . Experimental data in the panel (b) are taken from Marr et al. <sup>44</sup> and Southworth et al. <sup>45</sup> . . . . .	22
2	Photoionization cross section (a) and asymmetry parameter (b) for ionization of the $N_2^+ A^2\Pi$ state. The other details are the same as in Fig. 1. . . . .	23
3	Photoionization cross section (a) and asymmetry parameter (b) for ionization of the $N_2^+ B^2\Sigma_u^+$ state. The other details are the same as in Fig. 1. . . . .	24
4	Photoionization cross section (a) and asymmetry parameter (b) for ionization of the $N_2^+ 2^2\Sigma_g^+$ state. The symbol represents the cross section for the “Z” state of $N_2^+$ in Hamnett et al. <sup>41</sup> The other details are the same as in Fig. 1. . . . .	25
5	Photoionization cross section (a) and asymmetry parameter (b) for ionization of the $NO^+ X^1\Sigma^+$ state. Our CASSCF target results and SCF target results are represented as thick full lines and thick dashed lines, respectively. The previous theoretical results of Stratmann et al. <sup>25</sup> are shown as thin dashed lines. Experimental data in the figure are taken from Southworth et al. <sup>46</sup> and Iida et al. <sup>47</sup> . . . . .	26
6	Photoionization cross section (a) and asymmetry parameter (b) for ionization of the $NO^+ b^3\Pi$ state. The other details are the same as in Fig. 5. . . . .	27
7	Photoionization cross section (a) and asymmetry parameter (b) for ionization of the $NO^+ A^1\Pi$ state. The other details are the same as in Fig. 5. . . . .	28

8	Photoionization cross section (a) and asymmetry parameter (b) for ionization of the $\text{NO}^+ w^3\Delta$ , $a^3\Sigma^+$ , $A'^1\Sigma^-$ , $b'^3\Sigma^-$ and $W^1\Delta$ states, obtained by the R-matrix calculation in this work. The black dots indicate the experimental asymmetry parameter of Southworth et al. <sup>46</sup> averaged over these five $\text{NO}^+$ electronic states. ....	29
---	---	----

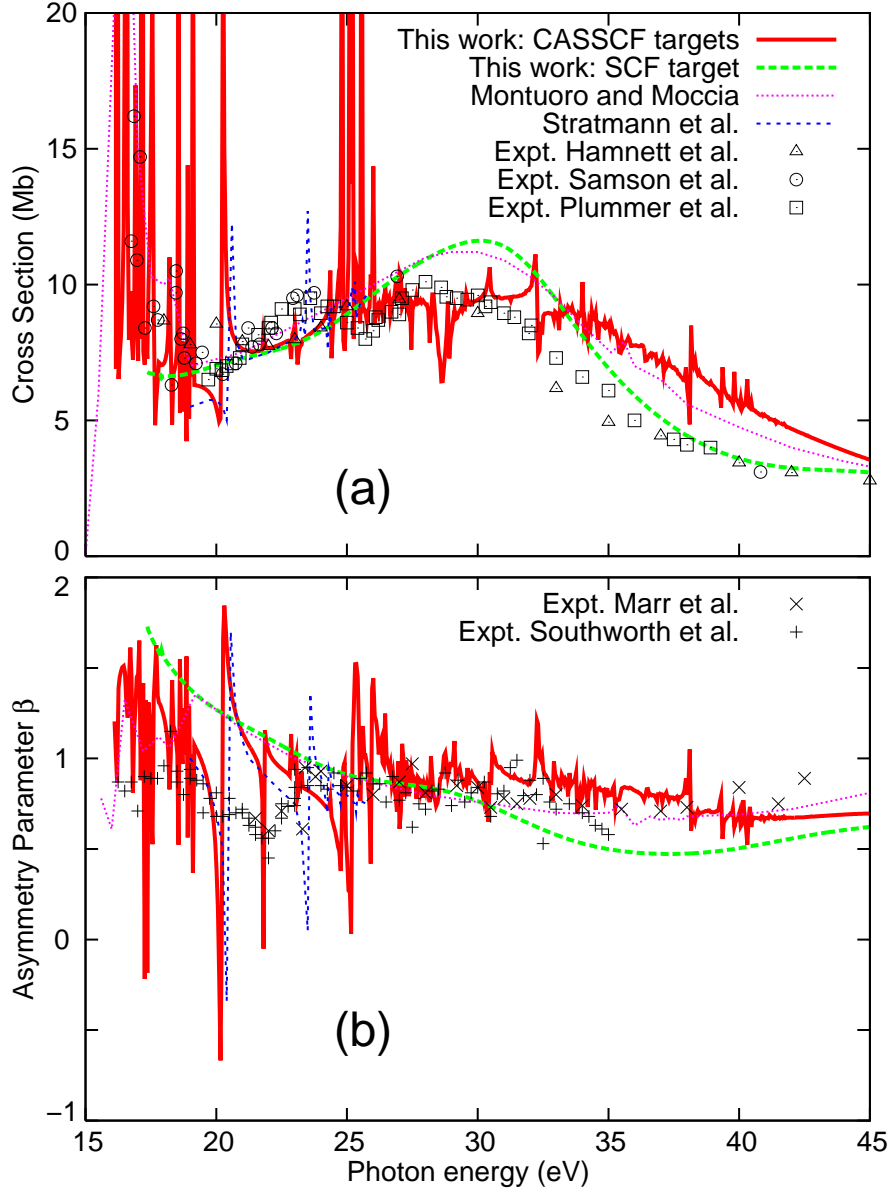


FIG. 1. Photoionization cross section (a) and asymmetry parameter (b) for ionization of the  $N_2^+ X^2\Sigma_g^+$  state. The cross sections are shown in unit of mega barn (Mb), equal to  $10^{-22}\text{m}^2$ . Our CASSCF target results and SCF target results are represented as thick full lines and thick dashed lines, respectively. The previous theoretical results of Montuoro and Moccia<sup>6</sup> and Stratmann et al.<sup>40</sup> are shown as thin dotted and thin dashed lines, respectively. Experimental data included in the panel (a) are taken from Hamnett et al.<sup>41</sup>, Samson et al.<sup>42</sup> and Plummer et al.<sup>43</sup>. Experimental data in the panel (b) are taken from Marr et al.<sup>44</sup> and Southworth et al.<sup>45</sup>

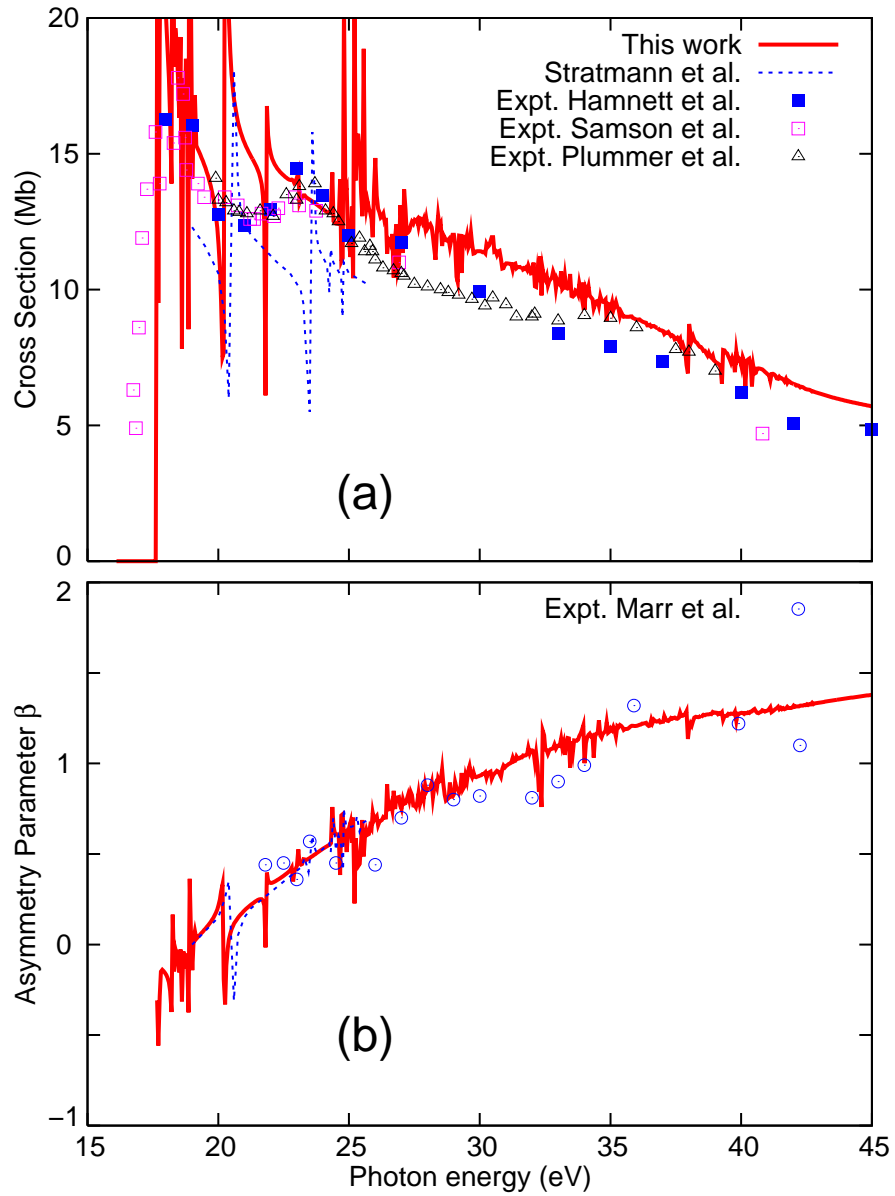


FIG. 2. Photoionization cross section (a) and asymmetry parameter (b) for ionization of the  $N_2^+ A^2\Pi$  state. The other details are the same as in Fig. 1.

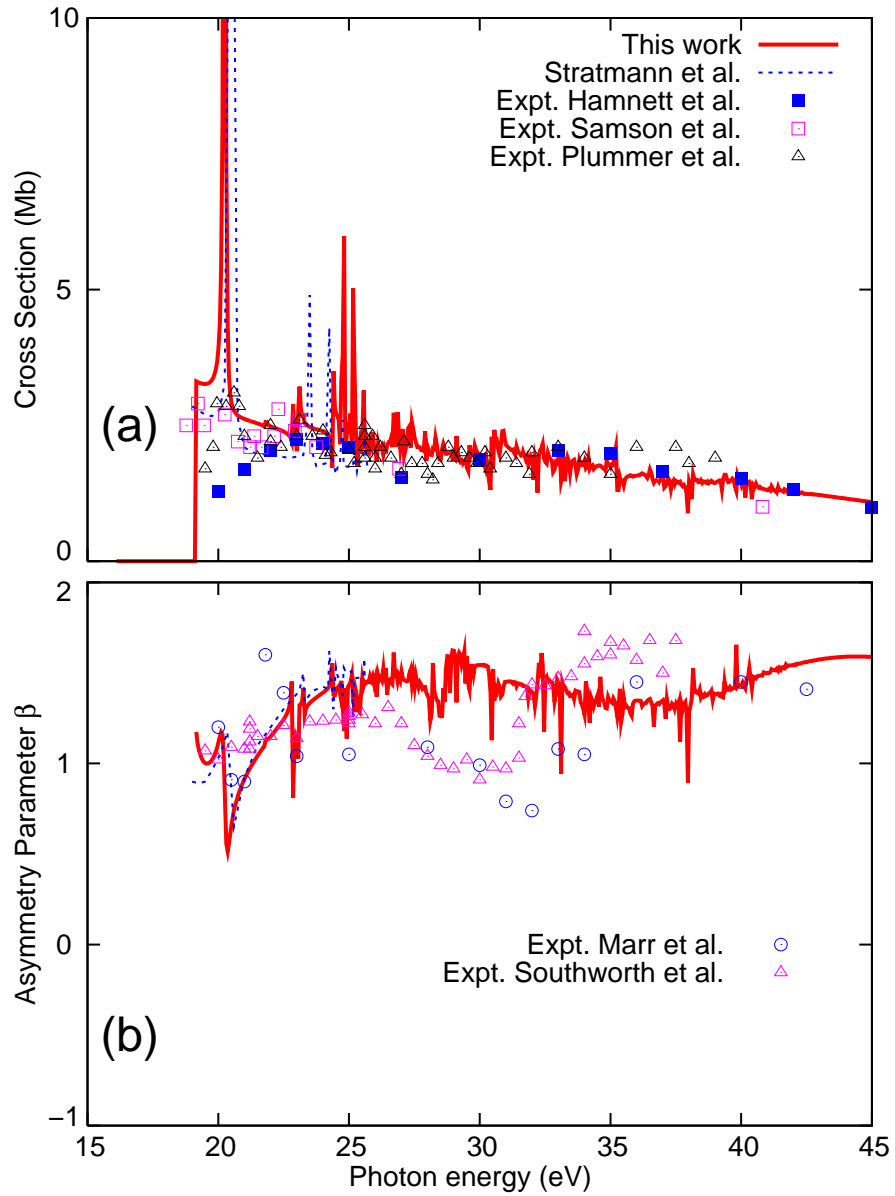


FIG. 3. Photoionization cross section (a) and asymmetry parameter (b) for ionization of the  $N_2^+ B^2\Sigma_u^+$  state. The other details are the same as in Fig. 1.



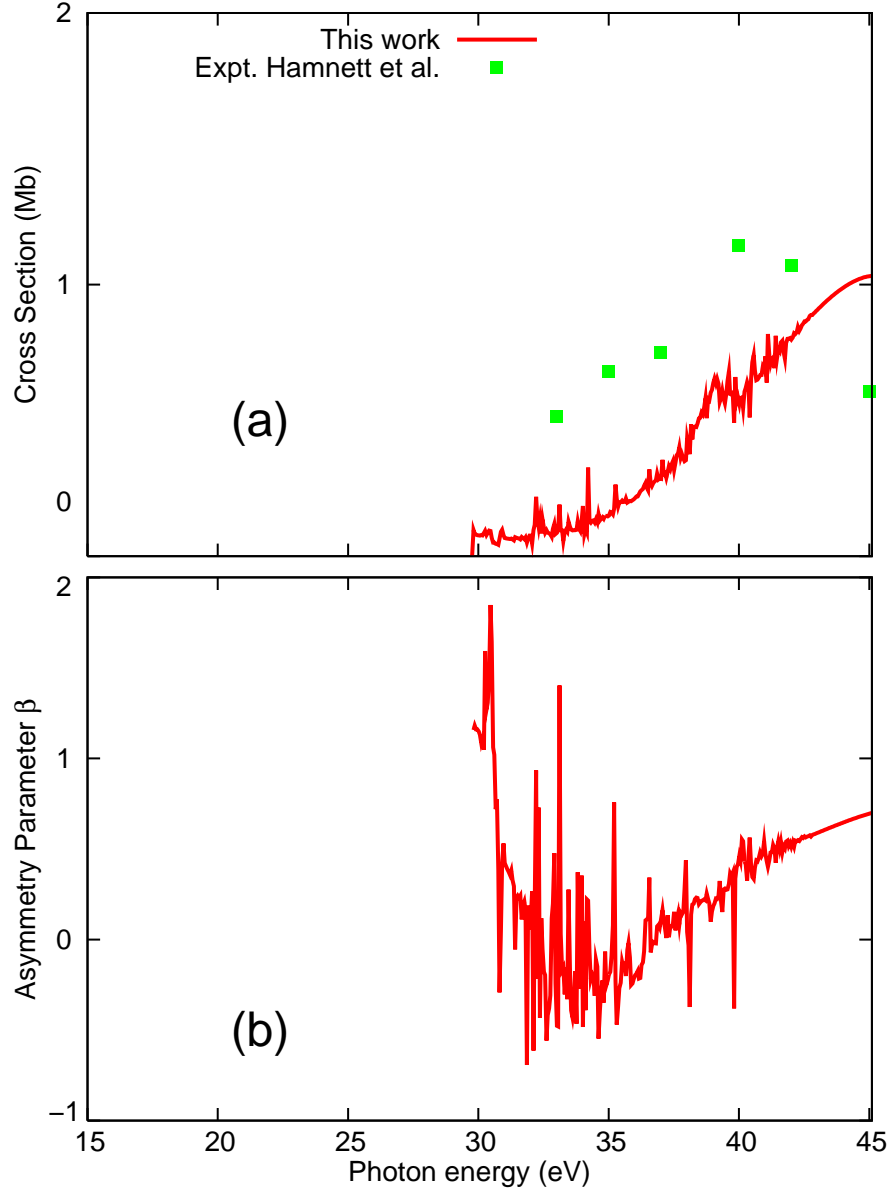


FIG. 4. Photoionization cross section (a) and asymmetry parameter (b) for ionization of the  $N_2^+ 2^2\Sigma_g^+$  state. The symbol represents the cross section for the “Z” state of  $N_2^+$  in Hamnett et al.<sup>41</sup> The other details are the same as in Fig. 1.

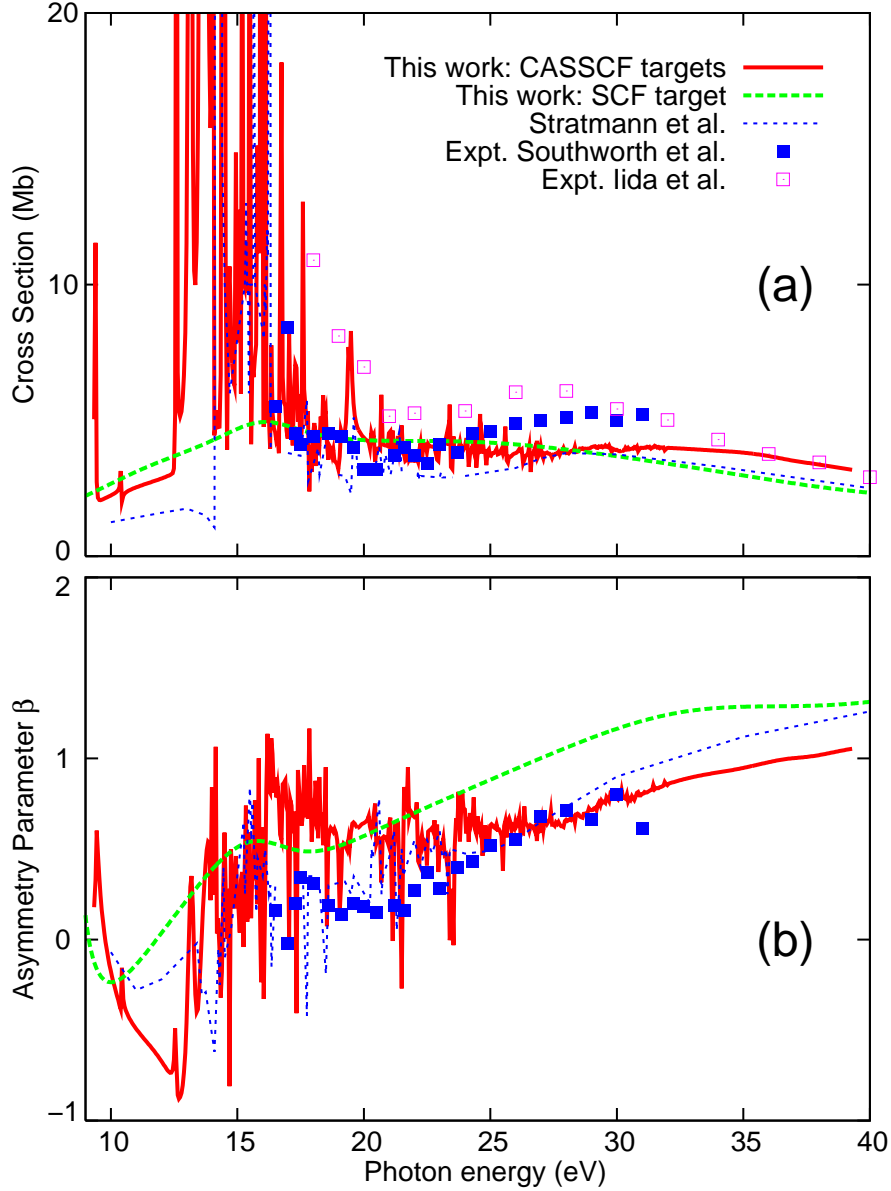


FIG. 5. Photoionization cross section (a) and asymmetry parameter (b) for ionization of the  $\text{NO}^+ X^1\Sigma^+$  state. Our CASSCF target results and SCF target results are represented as thick full lines and thick dashed lines, respectively. The previous theoretical results of Stratmann et al.<sup>25</sup> are shown as thin dashed lines. Experimental data in the figure are taken from Southworth et al.<sup>46</sup> and Iida et al.<sup>47</sup>

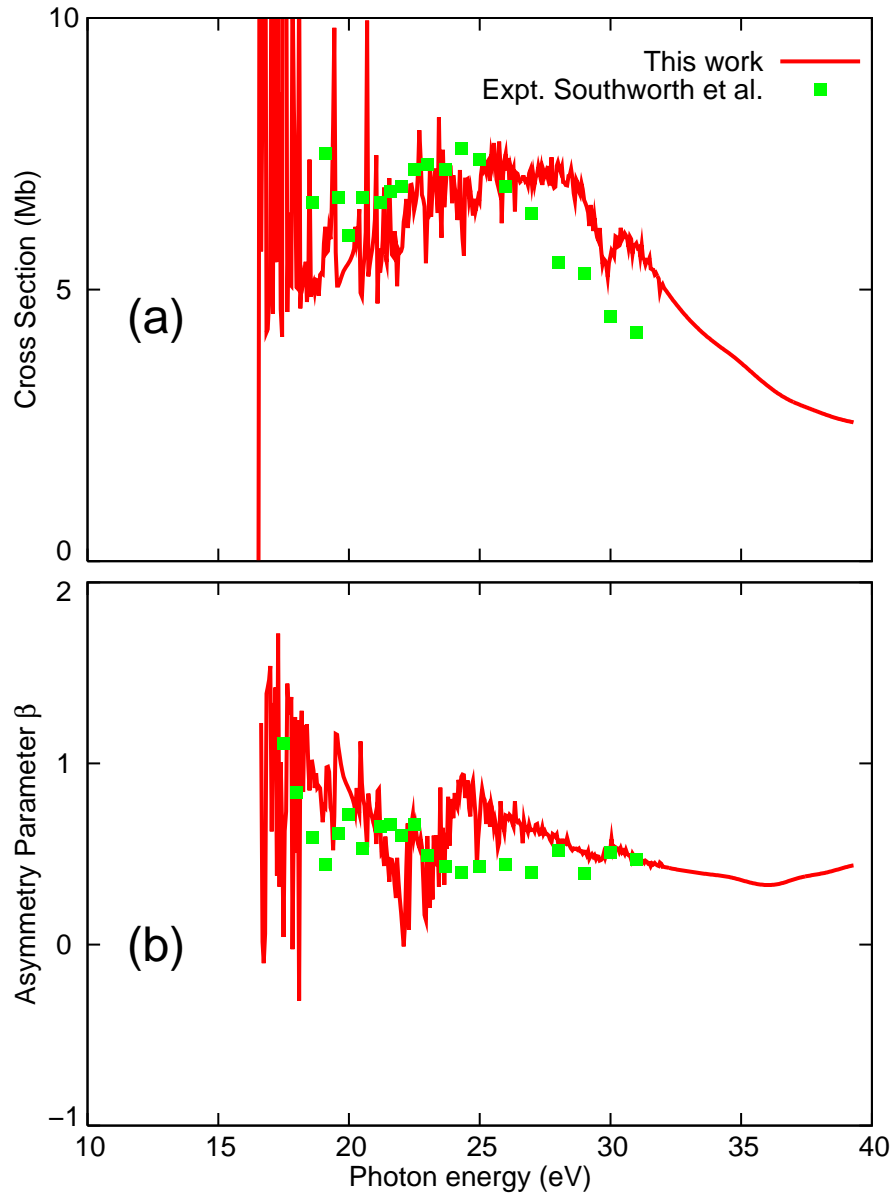


FIG. 6. Photoionization cross section (a) and asymmetry parameter (b) for ionization of the  $\text{NO}^+ b^3\Pi$  state. The other details are the same as in Fig. 5.

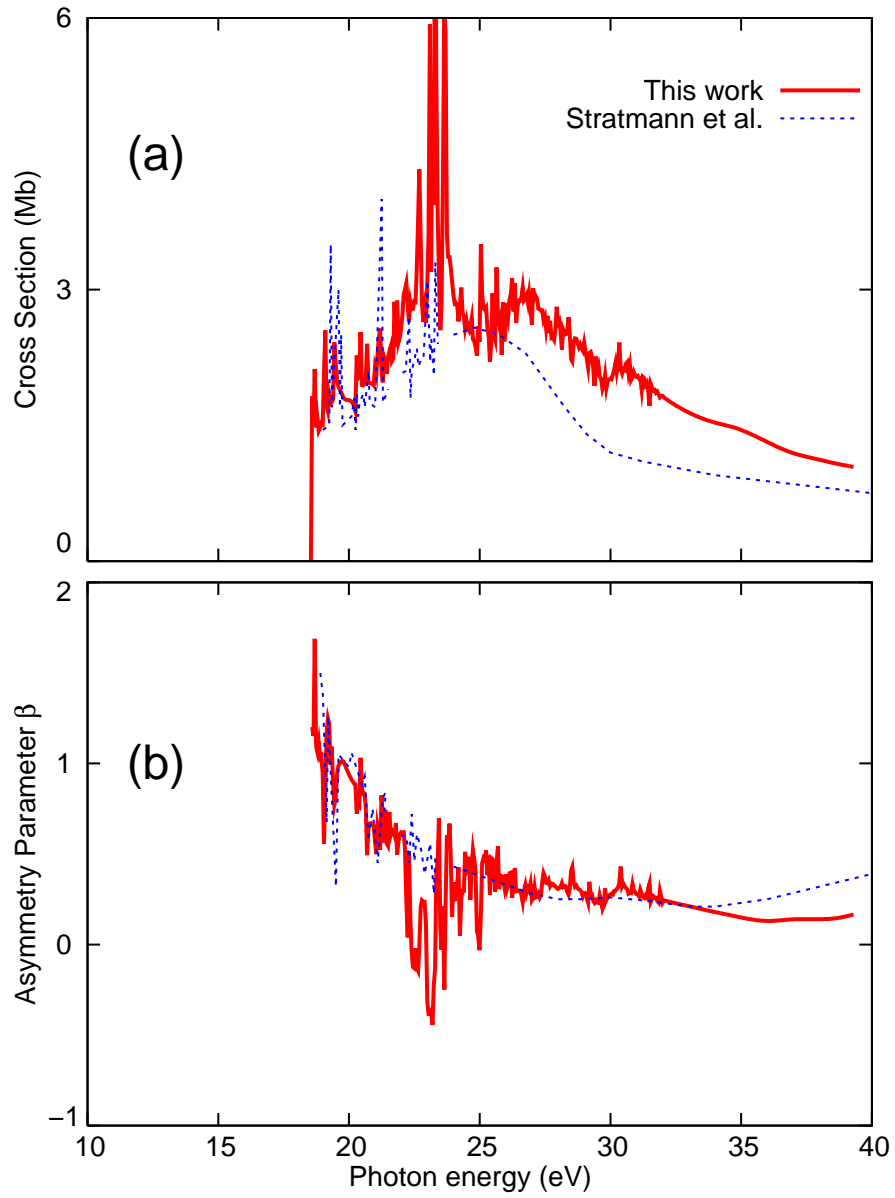


FIG. 7. Photoionization cross section (a) and asymmetry parameter (b) for ionization of the  $\text{NO}^+ A^1\Pi$  state. The other details are the same as in Fig. 5.

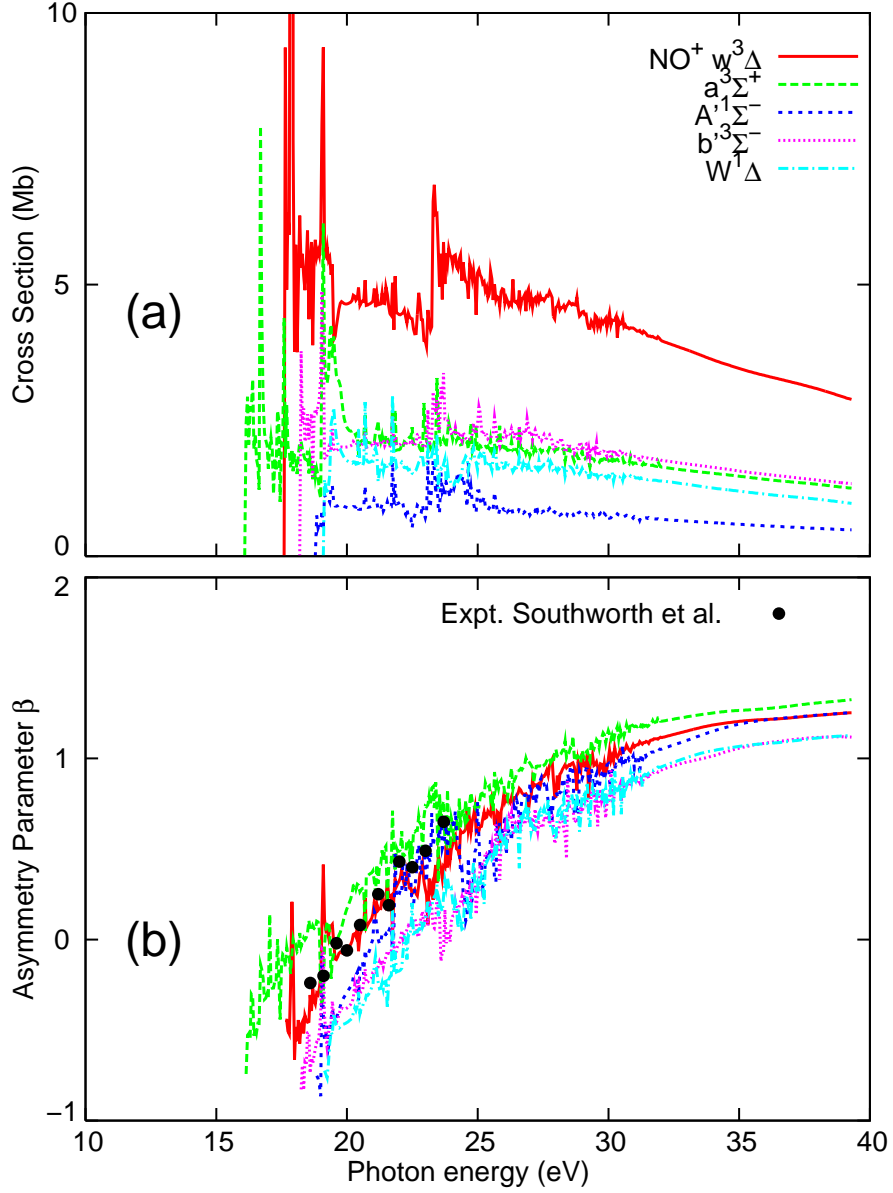


FIG. 8. Photoionization cross section (a) and asymmetry parameter (b) for ionization of the  $\text{NO}^+ w^3\Delta$ ,  $a^3\Sigma^+$ ,  $A'^1\Sigma^-$ ,  $b^3\Sigma^-$  and  $W^1\Delta$  states, obtained by the R-matrix calculation in this work. The black dots indicate the experimental asymmetry parameter of Southworth et al.<sup>46</sup> averaged over these five  $\text{NO}^+$  electronic states.

TABLE I. Vertical ionization potentials of N<sub>2</sub> molecule for the lower N<sub>2</sub><sup>+</sup> ionic states (eV). Experimental values are taken from Baltzer et al.<sup>38</sup>

N <sub>2</sub> <sup>+</sup> state	Main configuration	This work	Expt.
X <sup>2</sup> Σ <sub>g</sub> <sup>+</sup>	(3σ <sub>g</sub> ) <sup>-1</sup>	16.06	15.58
A <sup>2</sup> Π <sub>u</sub>	(1π <sub>u</sub> ) <sup>-1</sup>	17.64	16.93
B <sup>2</sup> Σ <sub>u</sub> <sup>+</sup>	(2σ <sub>u</sub> ) <sup>-1</sup>	19.13	18.75
D <sup>2</sup> Π <sub>g</sub>	(3σ <sub>g</sub> ) <sup>-2</sup> (1π <sub>g</sub> ) <sup>+1</sup>	25.60	24.79
C <sup>2</sup> Σ <sub>u</sub> <sup>+</sup>	(3σ <sub>g</sub> ) <sup>-1</sup> (1π <sub>u</sub> ) <sup>-1</sup> (1π <sub>g</sub> ) <sup>+1</sup>	26.35	25.51
2 <sup>2</sup> Π <sub>g</sub>	(1π <sub>u</sub> ) <sup>-2</sup> (1π <sub>g</sub> ) <sup>+1</sup>	27.06	26
1 <sup>2</sup> Σ <sub>u</sub> <sup>-</sup>	(3σ <sub>g</sub> ) <sup>-1</sup> (1π <sub>u</sub> ) <sup>-1</sup> (1π <sub>g</sub> ) <sup>+1</sup>	27.13	
1 <sup>2</sup> Δ <sub>u</sub>	(3σ <sub>g</sub> ) <sup>-1</sup> (1π <sub>u</sub> ) <sup>-1</sup> (1π <sub>g</sub> ) <sup>+1</sup>	27.26	
2 <sup>2</sup> Σ <sub>g</sub> <sup>+</sup>	(2σ <sub>u</sub> ) <sup>-1</sup> (1π <sub>u</sub> ) <sup>-1</sup> (1π <sub>g</sub> ) <sup>+1</sup>	29.65	

TABLE II. Ionization potentials of NO molecule for the lower NO<sup>+</sup> ionic states (eV). Our IPs are calculated for the vertical ionizations, while the experimental IPs taken from Albitton et al.<sup>39</sup> are for the adiabatic ionizations.

NO <sup>+</sup> state	Main configuration	This work	Expt.
$X^1\Sigma^+$	$(2\pi)^{-1}$	9.29	9.26
$a^3\Sigma^+$	$(1\pi)^{-1}$	16.13	15.66
$b^3\Pi$	$(5\sigma)^{-1}$	16.56	16.56
$w^3\Delta$	$(1\pi)^{-1}$	17.59	16.88
$b'^3\Sigma^-$	$(1\pi)^{-1}$	18.23	17.60
$A^1\Pi$	$(5\sigma)^{-1}$	18.55	18.33
$A'^1\Sigma^-$	$(1\pi)^{-1}$	18.81	17.82
$W^1\Delta$	$(1\pi)^{-1}$	19.10	18.08